

## Influence of heat input on the Charpy ductile fracture behavior of reheated HAZ in GMAW multilayer welded joints on HSLA steel using digital fractographic analysis

Benjamín Vargas-Arista<sup>a,✉</sup>, Oscar Mendoza-Camargo<sup>a</sup>, Irineo P. Zaragoza-Rivera<sup>a</sup>, Ariosto Medina-Flores<sup>b</sup>, Alberto Cuevas-Salgado<sup>a</sup>, Elizabeth Garfias-García<sup>c</sup>, Felipe García-Vázquez<sup>d</sup>

<sup>a</sup>Tecnológico Nacional de México, Instituto Tecnológico de Tlalnepantla, DEPI Av. Instituto Tecnológico s/n, Col. La Comunidad, Tlalnepantla de Baz, Estado de México, C.P. 54070, México

<sup>b</sup>Universidad Michoacana de San Nicolás de Hidalgo, Ciudad Universitaria, Morelia, Michoacan, México

<sup>c</sup>Departamento de Materiales, Area de Ingeniería de Materiales, División de CBI, UAM – Azcapotzalco, AV. San Pablo No. 180, Col. Reynosa Tamaulipas, Azcapotzalco, 02200, México, D.F.

<sup>d</sup>Facultad de Ingeniería de la Universidad Autónoma de Coahuila, Fundadores Km 13 Ciudad Universitaria, Arteaga, Coahuila, 25354, México

✉Corresponding author: [benvargasa@gmail.com](mailto:benvargasa@gmail.com)

Submitted: 21 July 2018; Accepted: 20 February 2019; Available On-line: 20 June 2019

**ABSTRACT:** The effect of the heat input on the fracture behavior of reheated heat affected zone in multi-layered welded joints of ASTM A633 steel was evaluated using the impact test, fractography, scanning electron microscopy and digital images processing. The impact results indicated a reduction in the Charpy energy as a function of the wire feed rate, which was confirmed by fractographs after digital images processing that showed a decrease in volumetric fractions of micro-dimples in ductile failures accompanying the increase in feed rate, favoring brittle fractures in transgranular cleavage facets containing river marks. The minimum fractions in micro-voids and the largest size of facets showing a higher number of river patterns were found at maximum feed rate of 200 mm·s<sup>-1</sup>. Heterogeneous microstructure of heat affected zone formed by fine acicular ferrite network surrounded by allotriomorphic ferrite showed that an increase in the feed rate induced a grain refinement by the formation of acicular ferrite, which was linked to the deterioration of absorbed energy and brittle failures.

**KEYWORDS:** Charpy energy; Digital Image Processing; Multi-layered GMAW process; Reheated HAZ

**Citation/Citar como:** Vargas-Arista, B.; Mendoza-Camargo, O.; Zaragoza-Rivera, I.P.; Medina-Flores, A.; Cuevas-Salgado, E.; Garfias-García, F.; García-Vázquez, F. (2019). "Influence of heat input on the Charpy ductile fracture behavior of reheated HAZ in GMAW multilayer welded joints on HSLA steel using digital fractographic analysis". *Rev. Metal.* 55(2): e143. <https://doi.org/10.3989/revmetalm.143>

**RESUMEN:** *Influencia del calor de entrada sobre el comportamiento a la fractura dúctil Charpy de la ZAC recalentada en uniones soldadas multipasos GMAW en acero HSLA utilizando análisis fractográfico digital.* El efecto del calor de entrada sobre el comportamiento a la fractura de la zona afectada por el calor recalentada en uniones soldadas multipasos de acero ASTM A633 fue evaluado mediante la prueba de impacto, fractografía, microscopía electrónica de barrido y procesamiento digital de imágenes. Los resultados de impacto indicaron una reducción en la energía Charpy como función de la velocidad de alimentación de alambre, lo cual se confirmó mediante fractografías después del procesamiento digital de imágenes que mostraron una reducción en la fracción volumétrica de microhuecos en la fractura dúctil acompañada del incremento en la rapidez de alimentación, favoreciendo la fractura frágil con facetas de clivaje transgranular conteniendo marcas de río. La fracción mínima de microhuecos y el tamaño más largo de facetas mostrando un mayor número de patrones de río fueron encontrados a la máxima rapidez de alimentación de 200 mm·s<sup>-1</sup>. La microestructura heterogénea de la zona afectada por el calor formada por una red de ferrita acicular fina rodeada por ferrita aliotromorfa mostro que el incremento en la rapidez de alimentación indujo un refinamiento de grano por la formación de ferrita acicular, lo cual se relacionó con el deterioro de la energía absorbida y fractura frágil.

**PALABRAS CLAVE:** Energía Charpy; Procesamiento digital de imagen; Proceso GMAW multipasos; ZAC recalentada

**ORCID ID:** Benjamin Vargas-Arista (<https://orcid.org/0000-0002-8210-9186>); Oscar Mendoza-Camargo (<https://orcid.org/0000-0002-7452-1402>); Irineo Pedro Zaragoza (<https://orcid.org/0000-0003-4858-6488>); Ariosto Medina (<https://orcid.org/0000-0002-9709-8790>); Alberto Cuevas-Salgado (<https://orcid.org/0000-0002-2234-2031>); Elizabeth Garfias-García (<https://orcid.org/0000-0001-7001-4967>); Felipe García-Vázquez (<https://orcid.org/0000-0003-2839-9650>)

**Copyright:** © 2019 CSIC. This is an open-access article distributed under the terms of the Creative Commons Attribution 4.0 International (CC BY 4.0) License.

## 1. INTRODUCTION

When planning the construction of a mining truck, an important factor that has to be taken into account is the impact behavior of the potential materials to be selected which could be welded, like high strength low alloy HSLA steel. In particular, ASTM A633 (2013) steel with well-defined weldability and moderate hardening could be proposed for use in the manufacturing of truck suspension parts. This steel can be joined using the gas metal arc welding (GMAW) process. A key outcome of this welding process is the formation of the heat affected zone (HAZ) with critical and deteriorated mechanical properties, formed by several complex heterogeneous microstructures after various weld beads using multi-pass welding (Furuya *et al.*, 2007; González *et al.*, 2010).

There has been some research on the mechanical and microstructural behavior of the HAZ, for example in ASTM A36M (2014) carbon steel using robotic GMAW process with different torch weaving modes (Guzmán *et al.*, 2017). Some works are related to the simulated coarse-grained HAZ for welded HSLA steel, which showed an evident decrease in fracture toughness with an increase in the size of the austenite grain and the volume fraction of martensite/austenite constituent distributed in a network (Shi and Han, 2008). In a second study of the degradation of fracture toughness in the inter-critically reheated coarse-grained HAZ in welded SN490 structural steel, the cracks with the lowest toughness were found to begin at the intersection of bainitic/ferrite followed by cleavage propagation resulting in a brittle fracture mechanism. In some areas of crack propagation adjacent cleavage facets are connected by shearing, thus producing dimple zones (Qiu *et al.*, 2000). Another example is the effect that normalizing at 1200 °C for 5 and 10 h has on grain size and the micro-hardness of weldments in shielding metal arc welding of AISI 4140 steel. For the HAZ normalized at 5 h, the microstructure showed idiomorphic and acicular ferrites. However, 10 h favored grain growth and Vickers hardness values decreased (12%) as related to the allotriomorphic ferrite containing acicular ferrite in large austenitic grains (Salazar-Garrido *et al.*, 2008).

On the other hand, where the automatic fracture analysis is concerned, research done in regards to digital processing on fractographs in fractures of weld bead aged at 250 °C for 500 and 900 h for welded joints in microalloy steel API5L-X52 was performed. The digital analysis on fractographic images was carried out using mathematical morphology and morphological transformation. The results indicated that the growth and coalescence of microcavities can be observed during the image segmentation (Mendoza *et al.*, 2013). Another investigation considered an image analysis routine

for the quantitative evaluation of the spatial distribution of particulate fillers in composite material. Micrographs of polished cross-sections were used as a base for binarization, noise-reduction and Voronoi-based tessellation operations, using open-source software. The cell area distributions were used to evaluate the microstructural homogeneity by their factor (Konegger, 2013). A study described the reconstruction of a failure using information obtained from pattern recognition in a digital fractographic analysis, taking into account quantitative features like the propagation of striations on the fracture surface. A new method called fractography by texture was developed, resulting in the calculation of variations in the load cycle for re-building the component failure (Nedbal *et al.*, 2008). One more investigation described a system for inspection of fractured surfaces using of multi-scale stereo-photogrammetry with images from scanning electron microscopy. This system facilitated the reconstruction of fractures in three dimensions resulting in a greater level of details and analysis of material behavior (Khokhlov *et al.*, 2012).

However, fewer contributions have been published on conventional or digital fractography (Guzmán *et al.*, 2017) under impact loads in reheated HAZ on steels such as ASTM A633 (2013). The objective of this investigation is to produce a clearer understanding of the causes and effects of impact fracturing, such as the degradation of the absorbed energy and microstructural zones. This work focused on the energy behavior in Charpy impact and fractographic analysis of the fracture surfaces on the HAZ generated by different wire feed rates in welded joints of the aforementioned steel. The relevance of this study is based on the fact that the HAZ is a detrimental hardened microstructural zone of lower toughness where cracks are nucleated in welded joints and are the core of degradation and failure in structural components. Also, the amount of the HAZ must be minimized by correct welding parameters to avoid cracks after a welding cycle according to the DIN EN 1011-2 (2001), which could drastically reduce the service life of welded joints. Therefore, the current study was necessary in order to improve the conventional fractographic and failure analysis using digital images processing and to reduce the uncertainty in fractographic parameters, like the volume fraction and density of micro-dimples or cleavage facets.

## 2. MATERIALS AND METHODS

### 2.1. Materials

Samples of welded joints with eight weld beads (250 mm in length, 250 mm in width and 12.7 mm in thickness) were obtained from plates of ASTM A633 (2013) low alloy steel which were welded

longitudinally using a GMAW-P process with a fillet configuration under welding procedure specification (WPS), including an AWS ER70S6 carbon steel electrode of 1.14 mm in diameter and using short circuit transfer mode with the bevel at 45° at both plates, a root opening of 9.52 mm, an inert gas mixture of 75% Ar / 25% CO<sub>2</sub> with a flow of 15 L·min<sup>-1</sup>, a travel speed of 33 cm·min<sup>-1</sup>, an arc voltage of 31 V, a fixed position 1G plane as per DIN EN 1011-2 (2001) and UNE EN ISO 15609-1 (2004). The GMAW process using different wire feed rates and heat inputs (Karadeniz *et al.*, 2007) was performed by a Miller semi-automatic power machining.

The chemical composition given for the filler and base metals in as-received conditions, as per AWS A5.18 (2005) and ASTM A633 (2013), respectively, is listed in Table 1. The values of carbon equivalent (C<sub>eq</sub>) were calculated by Eq. (1) from DIN EN 1011-2 (2001) and Easterling (1992) which complied with DIN EN 10025-2 (2004).

$$C_{eq} = C + \frac{Mn}{6} + \left( \frac{Cr + Mo + V}{5} \right) + \left( \frac{Cu + Ni}{15} \right) \quad (1)$$

The mechanical properties for weld and base metals are showed in Table 2, as per aforementioned ASTM Standard and AWS Specification. We observed that the weld bead exhibited greater mechanical resistance than the base metal, which complied with the basic design of welded joints.

## 2.2. Welding process

The semi-automatic GMAW-P process was performed using the two parameters (Karadeniz *et al.*, 2007) listed in Table 3, which can be represented by the heat input that was calculated by Eq. (2) and Eq. (3) (Atkins *et al.*, 2002) for each fillet welded joint, resulting in three different conditions.

$$Q_{net} = \eta Q_{arc} \quad (2)$$

Where:  $Q_{net}$  = net heat input (kJ·mm<sup>-1</sup>)  
 $\eta$  = heat transfer efficiency, 0.85 for GMAW process

$$Q_{arc} = \left( \frac{E I}{s} \right) 60 = \text{arc energy (kJ·mm}^{-1}) \quad (3)$$

Where: E = arc voltage (V)  
 I = welding current (A)  
 s = travel speed (cm·min<sup>-1</sup>)

## 2.3. Mechanical and microstructural characterization

Specimens of welded joints were characterized using microstructural analysis, Charpy impact tests (Teran *et al.*, 2017) and fractographic study. For the evaluation of microstructures, transversal specimens of 10 mm in width and 40 mm in length were used. The specimens were cut in work-pieces, were ground, polished with alumina, and subsequently etched using Nital 2% to reveal the microstructural zone to be studied. The microstructural features were observed using a Carl Zeiss Axiovert 40MAT optical microscope.

In order to characterize the impact energy of the reheated HAZ of the weld metal, sub-sized test pieces were machined to reduced type-A, rectangular cross sections, with transverse orientation, 7.5 mm thick, 10 mm wide, 55 mm long and V-notched at 45° located within the reheated HAZ between the weld beads. In order to assure the main part of the Charpy notch in the reheated HAZ, it was made

TABLE 3. GMAW welding parameters under study

Specimen	Welding current (A)	Wire feed rate (mm·s <sup>-1</sup> )	Net heat input $Q_{net}$ (kJ·mm <sup>-1</sup> )
P7	258	180	1.232
P8	272	190	1.299
P9	272	200	1.303

TABLE 1. Chemical composition of the ER70S6 filler metal and ASTM A633 base metal (Wt.%)

Material	C	Mn	Si	Cr	Ni	Mo	Cu	C <sub>eq</sub>
ER70S6	0.067	1.41	0.271	0.114	0.129	0.037	0.270	0.349
ASTM A633	0.179	0.973	0.239	0.411	0.164	0.170	0.178	0.474

TABLE 2. Mechanical properties of the micro-wire and base metal

Material	Vickers hardness HVN, 300 g <sub>f</sub>	Yield strength, $\sigma_y$ (MPa)	Ultimate tensile strength, $\sigma_u$ (MPa)	Elongation (%)	Charpy energy at -30 °C (J)
ASTM A633	183.9	416	509	24	154
ER70S6	209.3	473	579	21	75

the metallographic preparation of the transversal face of each specimen to have the marked localization of the notch before the machining process. Then, this marked location was the center of each impact specimen. A Charpy V-notch test was carried out using an Otto Wolpert-Werke pendulum impact machine, type PW 30/15 K at  $-30\text{ }^{\circ}\text{C}$  in triplicate, in accordance with ASTM E23 (2016).

The fractography of the impact fractured specimens was performed by a Carl Zeiss –Gemini Supra 55 VP scanning electron microscope (SEM). The fractographs were obtained using a secondary electron signal, 10 kV, 220  $\mu\text{A}$ , and a work distance of 10 mm.

#### 2.4. Digital image processing (DIP)

This processing was applied to quantify the fractographic features of the fractographs using mathematical morphology and morphological transformation. The DIP has important applications in failure analysis through the fractographic digital processing of fracture surfaces using mathematical morphology, a potent tool in DIP because it can quantify several features of the geometrical structures of the images in a manner similar to the way human intuition. Top-Hat transformation is an operation of morphologic transformation which allows the extraction of the narrow bright zones of image in grayscale. These zones disappear after the aperture operation. For the structure of element B, the Top-Hat transformation of function  $f$  was defined in Eq. (4):

$$T_dFB(f) = f - (f)B \quad (4)$$

Where  $(f)_B$  represents the aperture operation. This transformation extracts the residuals zones of the aperture operation with  $f$  being the sizes of these zones that are smaller than the structure element B. Here B is chosen to be a convex set. For this study, a disc was applied as the structure element, and a lineal structure element with different orientations was used to more adequately determine the regions that could be extracted (Mendoza *et al.*, 2013).

### 3. RESULTS AND DISCUSSION

The semi-automatic welded joints of ASTM A-633 (2013) HSLA steel obtained at a greater heat input and a higher wire feed rate exhibited lower Charpy impact energy in the reheated HAZ of the weld metal, as well as greater flat area of mixed-fracture surfaces showing mainly brittle fracture in transgranular cleavage with bigger facets, containing well-defined river patterns and a reduction of small micro-hollows distributed throughout the surface (Mendoza *et al.*, 2013; Guzmán *et al.*, 2017). This impact fracture behavior was linked to

the microstructural features of a fine network of fine acicular ferrite (Thewlis, 2004; Wan *et al.*, 2010; Guzmán *et al.*, 2017) surrounded by allotriomorphic ferrite, which changed in size and amount as a consequence of the increase in wire rate.

#### 3.1. Charpy V-notch impact test

The variation in Charpy absorbed energy in different wire feed rates for the reheated HAZ is illustrated in the graph in Fig. 1. The effect of this rate was a significant reduction in the fracture energy when the wire rate was increased, i.e., with the minimum energy reduction being obtained at maximum rate of  $200\text{ mm}\cdot\text{s}^{-1}$ . The latter was obtained as a consequence of the highest heat input generated after GMAW welding thermal multi-cycles, which can be explained as a result of the maximum welding current. In the results obtained, the reheated HAZ showed a reduction of 62% in Charpy energy at  $200\text{ mm}\cdot\text{s}^{-1}$ , i.e., this HAZ absorbed a smaller amount of energy, compared to that of the initial sample obtained at  $180\text{ mm}\cdot\text{s}^{-1}$ . Consequently, the fracture energy (toughness) was shown to be strongly susceptible to the wire feed rate.

#### 3.2. Experimental fractography

The reduction in impact energy was confirmed using conventional fractographic analysis of the impact fractured surfaces of the reheated HAZ, obtained under different wire feed rates. At macroscopic level (Fig. 2), a central area with a granular morphology and brilliant surface was observed. This area increased in size as a function of the increase in wire rate. At  $180\text{ mm}\cdot\text{s}^{-1}$ , the fractured surface showed a nearly-planar central zone limited in size including a bright band at the end of the surface (Fig. 2a). As the wire feed increased to

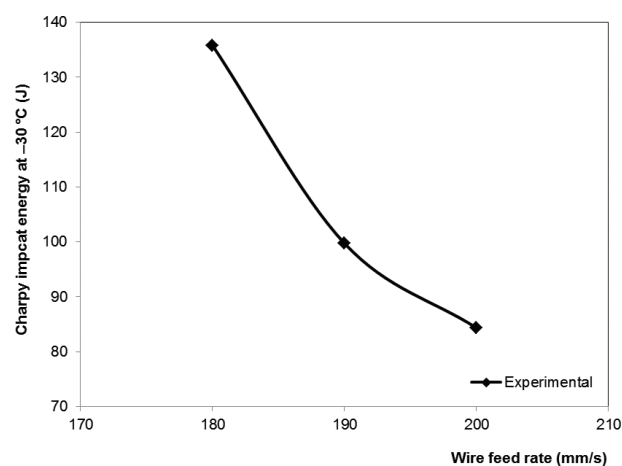


FIGURE 1. Charpy energy as a function of the wire feed rate for the reheated HAZ in GMAW welded joints.

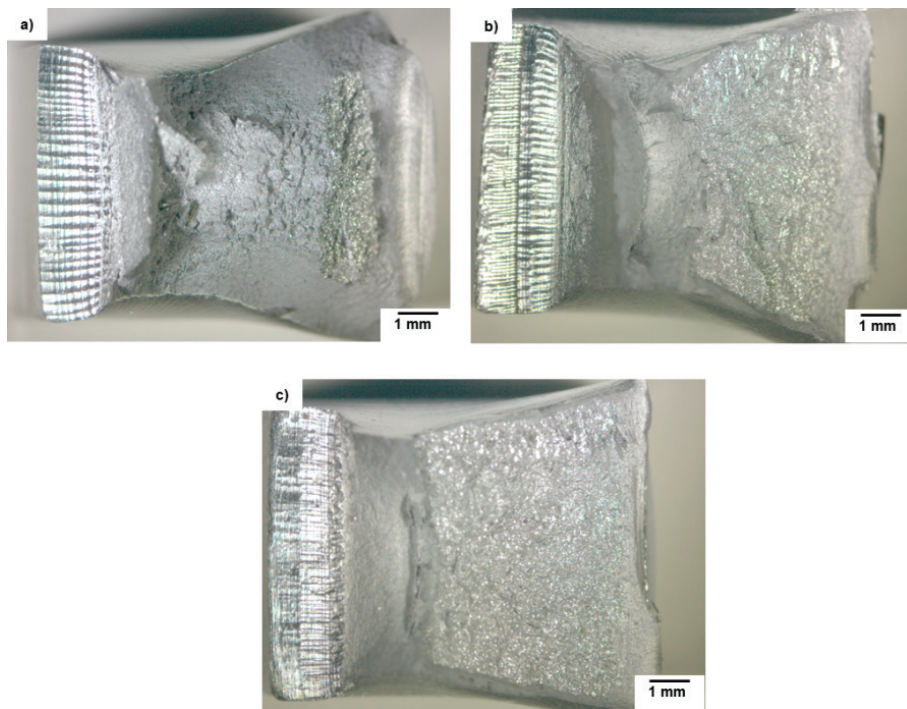


FIGURE 2. Macro-fractography of impact fractured specimens for reheated HAZ at different wire rates: a) surface with granular central zone at  $180 \text{ mm}\cdot\text{s}^{-1}$ , b) zone with greater planicity at  $190 \text{ mm}\cdot\text{s}^{-1}$ , and c) granular zone showing the largest size at  $200 \text{ mm}\cdot\text{s}^{-1}$ .

$190 \text{ mm}\cdot\text{s}^{-1}$ , this zone grew in size, covering a larger surface area with a planar granular appearance and higher brilliance, see Fig. 2b. At  $200 \text{ mm}\cdot\text{s}^{-1}$ , this zone reached its largest extension, covering the greatest fracture area with more brightness and planicity on the surface, as can be seen in Fig. 2c. The brilliance and granular appearance of the planar central zone, in differing sizes, could be associated with the fractographic features of the typical brittle fracture.

From the observations made on the fractographs obtained by SEM from impact fractured surfaces, we observed that the fracture was mainly brittle with well-defined transgranular facets containing river patterns in the direction of propagation, as well as minimum ductile fracture representing by microvoid bands (Guzmán *et al.*, 2017) within the surface and surrounding these facets. These fractographic features confirmed that the brittle fracture was made by cleavage. We also found that the cleavage facet size increased and the number of microvoids decreased, as a consequence of the wire feed rate, resulting in an increase in the number of river patterns within the cleavage facets with bigger size. At  $180 \text{ mm}\cdot\text{s}^{-1}$ , we observed facets of smaller sizes and a larger number of microhollows networks (Fig. 3a). At  $190 \text{ mm}\cdot\text{s}^{-1}$ , the number of microvoids clearly decreased while the facets increased in size (Fig. 3b). However, at  $200 \text{ mm}\cdot\text{s}^{-1}$  the transgranular cleavage

facets reached the largest size and had well-defined river patterns while the microdimples decreased in amount, see Fig. 3c.

According to the aforementioned fractographic features, and as part of the conventional fracture analysis, the number of cleavage facets and microvoid bands (Guzmán *et al.*, 2017) was directly measured on the fractographs and was reported as the volume fraction. It was observed that this fraction of transgranular cleavage facets slightly increased as a consequence of the increase in the wire rate (Fig. 4a), in relation to higher heat input. On the other hand, in Fig. 4b we see that the volume fraction of microhollows (Mendoza *et al.*, 2013; Guzmán *et al.*, 2017) clearly decreased as a function of the wire rate which we associated with the drastic reduction in absorbed energy. The largest reduction of microvoids (54%) was reached at  $200 \text{ mm}\cdot\text{s}^{-1}$  compared to those at the initial rate.

### 3.3. Digital image processing (DIP)

The DIP of the Charpy impact fractured surfaces (Fig. 5) was used to generate the digital fractography (Mendoza *et al.*, 2013). It was observed that the surface was composed in a scale of white to black, where black zones are the ductile fractures while bright white zones represent brittle fractures, which increased in size as a function of the

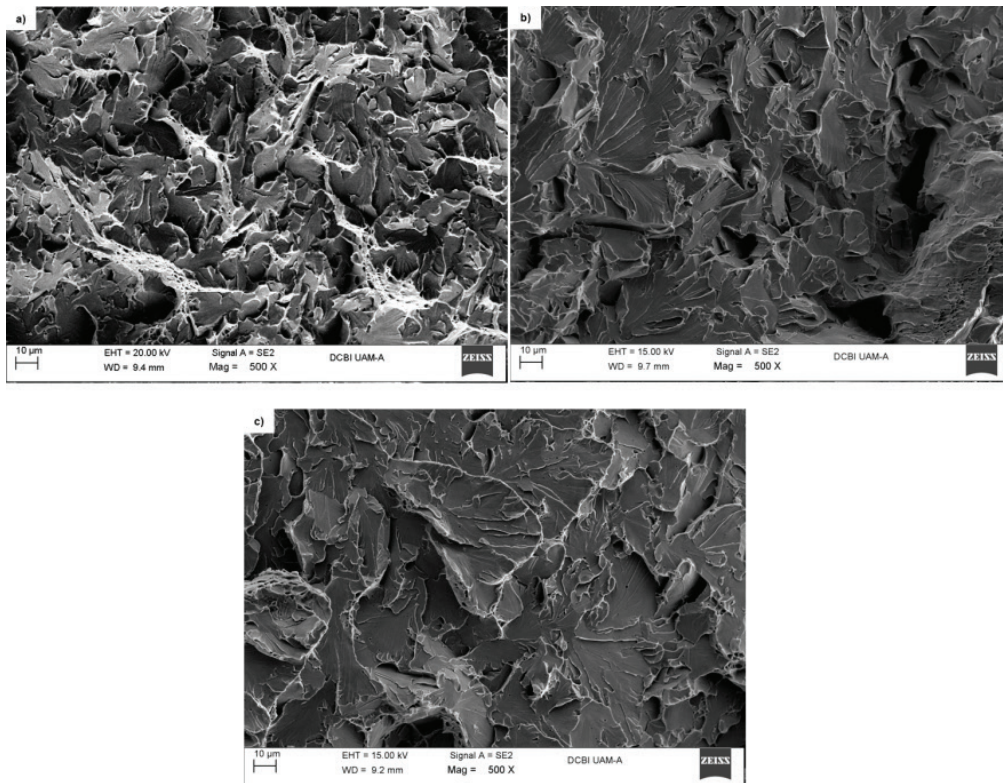


FIGURE 3. Digital fractography of impact fractured specimens for reheated HAZ at different wire rates: a) small cleavage facets at  $180 \text{ mm}\cdot\text{s}^{-1}$ , b) medium facets at  $190 \text{ mm}\cdot\text{s}^{-1}$ , and c) larger facets with river patterns at  $200 \text{ mm}\cdot\text{s}^{-1}$ .

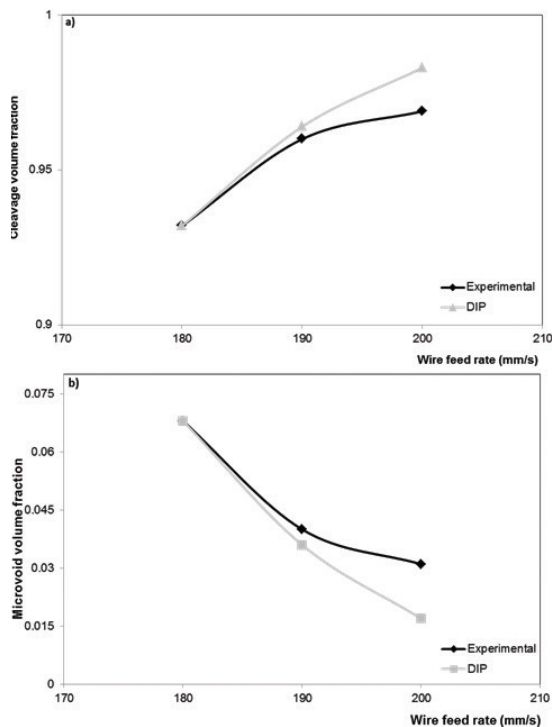


FIGURE 4. Volume fraction of: a) cleavage facets and b) microvoids as a function of wire feed rate for impact fractured specimens of reheated HAZ.

wire rate. At  $180 \text{ mm}\cdot\text{s}^{-1}$ , the central zone showed a higher amount of black tones (ductile failure), see Fig. 5a. At  $190 \text{ mm}\cdot\text{s}^{-1}$ , the black scale decreased, resulting in a greater amount of white scale representing a higher amount of brittle fracture (Fig. 5b). However, at  $200 \text{ mm}\cdot\text{s}^{-1}$ , the amount of white scale was the highest, which was linked to larger central planar zone of brittle fracture per cleavage (Fig. 5c). This DIP of the Charpy fractures was in agreement with the results from experimental fractography as described in section 3.2. Moreover, the average volume fraction of the central brittle zone for the three feed rates was measured using DIP, resulting in mean values which increased as a function of the increase in wire rate (Fig. 5d). The greatest increase in this central zone (91%) was reached at  $200 \text{ mm}\cdot\text{s}^{-1}$  compared to those at the initial condition.

Additionally, the digital fractography was produced by the DIP (Mendoza *et al.*, 2013) from the impact fractured surfaces (Fig. 6). We clearly observed well-defined black areas linked to a microvoids network of ductile fracture (Mendoza *et al.*, 2013; Guzmán *et al.*, 2017) which was reduced as a consequence of the increase in wire rate. At  $180 \text{ mm}\cdot\text{s}^{-1}$ , these black zones appeared in significant amounts on the surface, and were associated with small and medium sizes of microdimples, see Fig. 6a. At  $190 \text{ mm}\cdot\text{s}^{-1}$ , the number of black

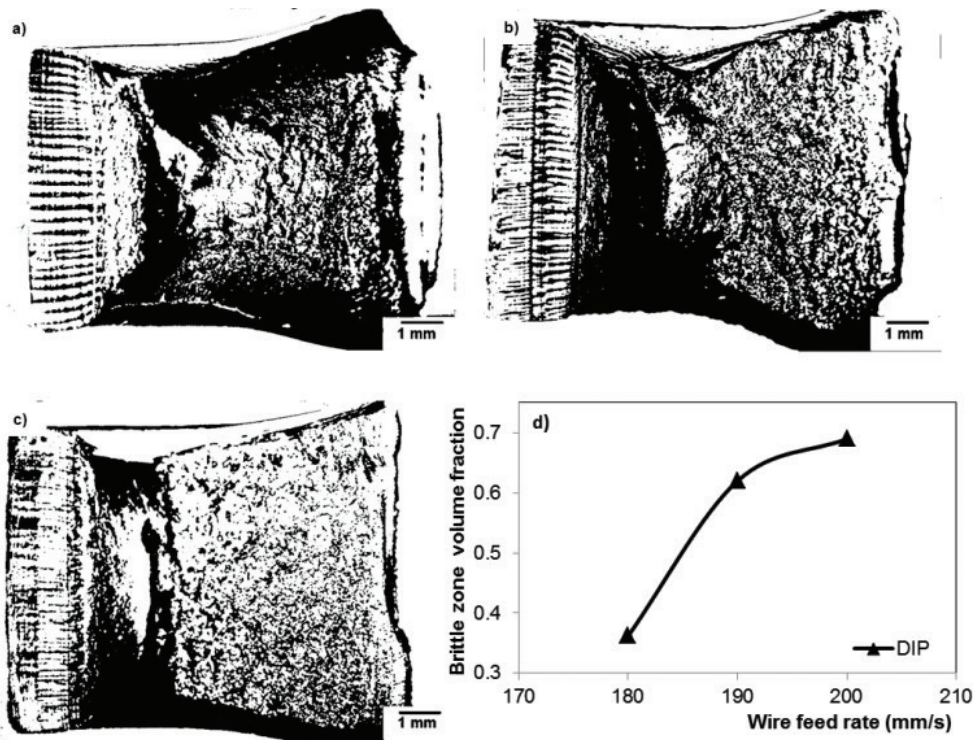


FIGURE 5. Segmented images obtained by DPI for impact fractured surface of reheated HAZ with different wire feed rates: a) rough white-black central zone at  $180 \text{ mm}\cdot\text{s}^{-1}$ , b) semi-planar central zone at  $190 \text{ mm}\cdot\text{s}^{-1}$ , c) bright white planar central zone at  $200 \text{ mm}\cdot\text{s}^{-1}$ , and d) volume fraction of central zone vs. wire feed rate.

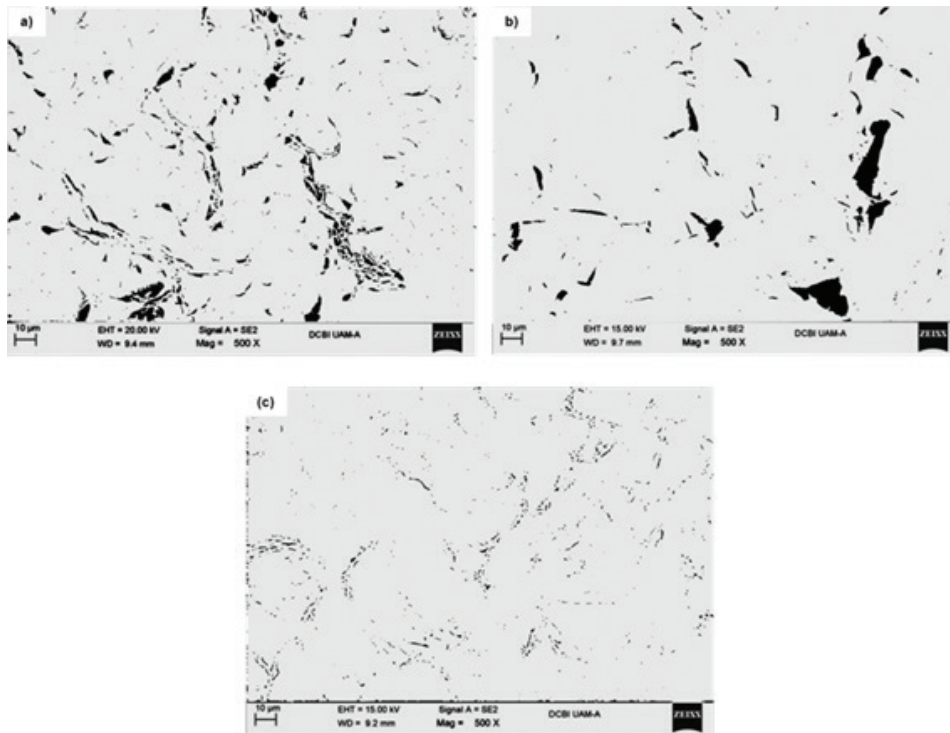


FIGURE 6. Segmented images obtained by DPI for impact fractured surface of reheated HAZ with different wire rates: a) black zones show a microdimple network at  $180 \text{ mm}\cdot\text{s}^{-1}$ , b) straight lines show secondary cracking at  $190 \text{ mm}\cdot\text{s}^{-1}$ , and c) minimum black areas at  $200 \text{ mm}\cdot\text{s}^{-1}$ .

regions (microvoid networking) was reduced. An interesting DIP result was that there were straight black lines related to secondary cracking very different from the round shape of microvoids (Fig. 6b). Finally at  $200 \text{ mm}\cdot\text{s}^{-1}$ , the amount of very fine black areas (representing microhollows) on the surface was clearly decreased, as can be seen in Fig. 6c. Then, the largest reduction of these black regions (75%) and therefore microdimples was reached at latter rate, compared to those at the initial condition.

Moreover, the DIP technique was applied to quantify the volume fraction of the cleavage facets (Fig. 4a), the microvoids (Fig. 4b) and to compare them to direct measurements, resulting in similar values and tendencies for both fractions as a function of the wire feed rate, showing adequate agreement between digital and conventional fractography. The aforementioned impact fracture behavior could be linked to the microstructural features found, as will be explained in the next section.

### 3.4. Microstructural analysis

According to the optical microscopy observations on the three different welded joints, at a rate of  $180 \text{ mm}\cdot\text{s}^{-1}$  (Fig. 7a), the reheated HAZ between weld beads showed a microstructure composed of large allotriomorphic ferrite within the austenitic grain boundaries containing acicular ferrite (Thewlis, 2004; Guzmán *et al.*, 2017), which their amount was measured as volume fraction resulting the values reported in Fig. 8. At  $190 \text{ mm}\cdot\text{s}^{-1}$ , the volume fraction of acicular ferrite increased (16%) and medium size allotriomorphic ferrites were observed (Fig. 7b). However at  $200 \text{ mm}\cdot\text{s}^{-1}$ , there was a notable grain refinement by the formation of the largest volume fraction (26%) of acicular ferrite network (Wan *et al.*, 2010) and fine allotriomorphic ferritic grains, see Fig. 7c.

Therefore, there were similar microstructures with differences in volume fraction of acicular ferrite (Fig. 8) and sizes of allotriomorphic ferritic grains for the reheated HAZ generated at the three

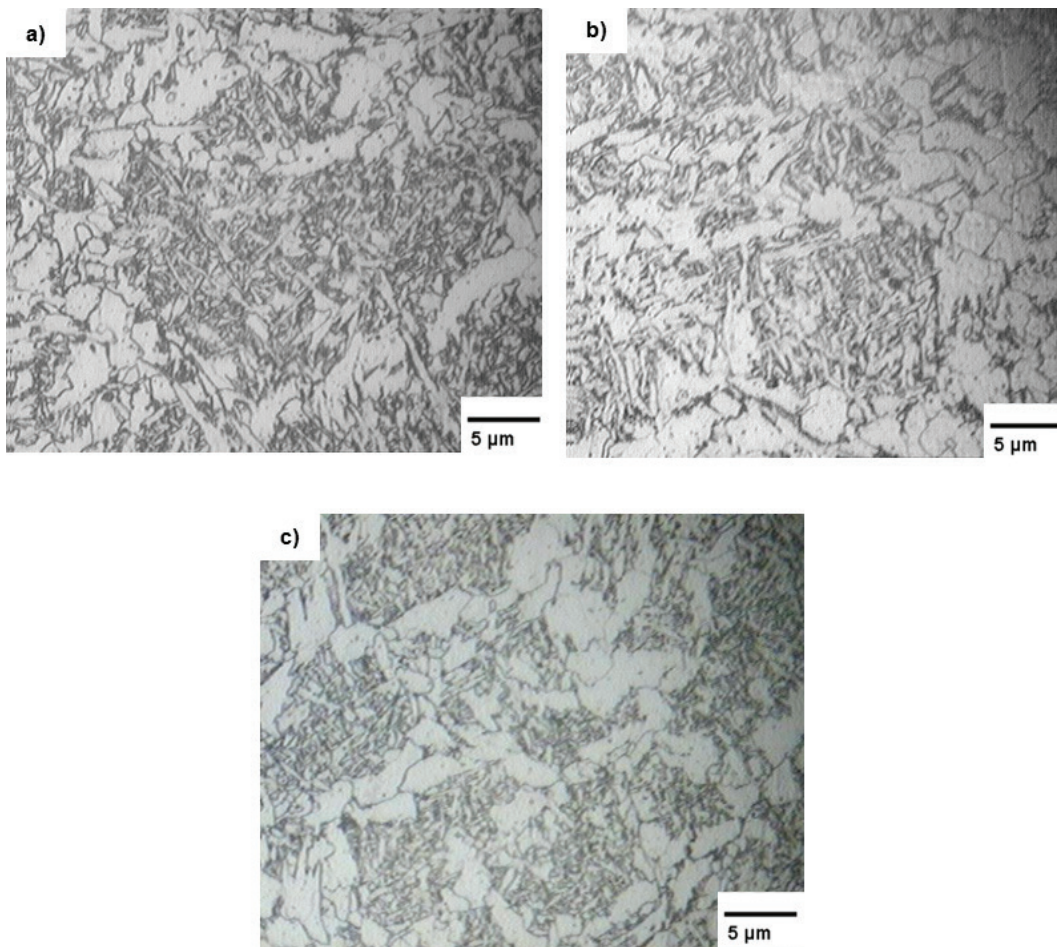


FIGURE 7. Optical micrographs obtained from the reheated HAZ at different wire rated: a) acicular ferrite at  $180 \text{ mm}\cdot\text{s}^{-1}$ , b) a higher volume fraction of acicular ferrite at  $190 \text{ mm}\cdot\text{s}^{-1}$ , and c) grain refinement of acicular ferrite network at  $200 \text{ mm}\cdot\text{s}^{-1}$ .

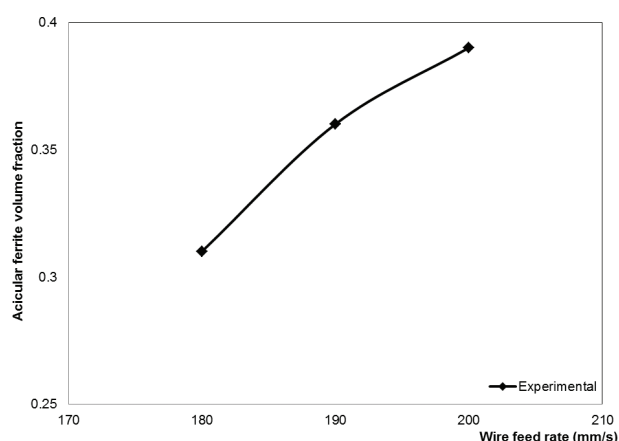


FIGURE 8. Volume fraction of acicular ferrite vs. wire feed rate from the reheated HAZ specimens.

different rates. Moreover, the effect of the increase in wire rate on the critical microstructures of this reheated HAZ was a grain refinement by acicular ferrite formation (Wan *et al.*, 2010) which was linked to a hardening (González *et al.*, 2010). Finally, this ferritic grain refinement favored the decrease in the impact absorbed energy (toughness) of the reheated HAZ of the weld metal as a consequence of the increase in the heat input values, which was linked to higher wire feed rate and welding current.

#### 4. CONCLUSIONS

The reheated HAZ of the weld metal in the fillet welded joints obtained by semi-automatic gas metal arc welding process with a greater net heat input, due to a higher welding current and wire feed rate, showed three notable changes analyzed by the digital image processing of fractographs; including brittle fracture by cleavage, reduction in Charpy energy and grain refinement by the formation of acicular ferrite network. The degradation of absorbed impact energy was linked to the reduction in the volume fraction of the microhollows network within the impact fractured surfaces, as a function of the increase in the wire rate. The latter increment favored an increase in the size of transgranular cleavage facets on the brittle fractures within the impact fractured surfaces, which was linked to the deterioration of the impact energy. The effect of higher rate with major heat input on the microstructure was a refinement of acicular ferrite grains networking within the reheated HAZ, which affected the Charpy energy values, aforementioned impact fracture behavior and caused greater susceptibility for cracking, which would affect the joint weldability. The digital image processing could be a better technique that conventional fractography for quantifying the significant fractographic features within impact fractured surfaces of reheated HAZ,

exhibiting brittle fracture by cleavage with larger facets and lower volume fraction of microhollows network at a higher heat input.

#### ACKNOWLEDGMENTS

The authors wish to thank ESQIE-Instituto Politécnico Nacional and laboratorio de microscopía electrónica de la división de CBI en la Universidad Autónoma Metropolitana Unidad Azcapotzalco for the experimental support received.

#### REFERENCES

- ASTM A633 (2013). *Standard specification for normalized high strength low alloy structural steel plates*. ASTM International, West Conshohocken, PA, USA, pp. 1–3.
- ASTM A36M (2014). *Standard specification for carbon structural steel*. ASTM International, West Conshohocken, PA, USA, pp. 1–3.
- ASTM E23 (2016). *Standard test methods for notched bar impact testing of metallic materials*. ASTM International, West Conshohocken, PA, USA, pp. 2–8.
- Atkins, G., Thiessen, D., Nissley, N., Adonyi, Y. (2002). Welding process effects in weldability testing of steels. *Weld. J.* 61–66. <http://img2.aws.org/wj/supplement/04-2002-ATKINS-s.pdf>.
- AWS A5.18 (2005). *Specification for carbon steel electrodes and rods for gas shielded arc welding*. American Welding Society, Miami FL, USA, pp. 2–6.
- DIN EN 1011-2 (2001). *Recommendations for welding of metallic materials, Part 2: Arc Welding of ferritic steels*. Deutsches Institut für Normung, Germany, p. 9.
- DIN EN 10025-2 (2004). *Hot rolled products of structural steels, part 2: technical delivery conditions for non-alloy structural steels*. Deutsches Institut für Normung, Germany, pp. 18–29.
- Easterling, K. (1992). *Introduction to the physical metallurgy of welding*. 2nd ed., Ed. Butterworths, London, England, pp. 1–54.
- Furuya, H., Aihara, S., Morita, K. (2007). A new proposal of HAZ toughness evaluation method - Part 1: HAZ toughness of structural steel in multilayer and single-layer weld joints. *Weld. J.* 86 (1), 1s-8s.
- González, G.S., Vargas, A.B., Solís, J., García, V.F. (2010). Effect of wire feed rate on the microstructure and microhardness of multilayer weldment by GMAW process on ASTM A633 steel. *32th Congreso Internacional de Metalurgia y Materiales*, Saltillo, Coahuila, México, pp. 1–11.
- Guzmán, F.I., Vargas, A.B., Gasca, D.J.J., Cruz, G.C.E., González, A.M., Del Prado, V.J. (2017). Effect of torch weaving on the microstructure, tensile and impact resistances, and fracture of the HAZ and weld bead by robotic GMAW process on ASTM A36 steel. *Soldagem & Inspeção* 22 (1), 72–86. <https://dx.doi.org/10.1590/0104-9224/si2201.08>.
- Karadeniz, E., Ozsarac, U., Yıldiz, C. (2007). The effect process parameters on penetration in gas metal arc welding processes. *Mater. Design* 28 (2), 649–656. <https://doi.org/10.1016/j.matdes.2005.07.014>.
- Khokhlov, M., Fischer, A., Rittel, D. (2012). Multi-scale stereophotogrammetry system for fractographic analysis using scanning electron microscopy. *Exp. Mech.* 52 (8), 975–991. <https://doi.org/10.1007/s11340-011-9582-0>.
- Konegger, T. (2013). Image-analytical evaluation of the spatial distribution of particulate fillers in ceramic composites prepared via the polymer-derived ceramics route. *Mater. Charact.* 86, 9–20. <https://doi.org/10.1016/j.matchar.2013.09.003>.
- Mendoza, O., Vargas, B., Mendoza, J. (2013). Digital processing of fractographic images for welded joints on microalloy steel API 5L X52 aged. *IEEE Lat. Am. T.* 11 (1), 172–176. <https://doi.org/10.1109/TLA.2013.6502798>.

- Nedbal, I., Siegl, J., Kunz, J., Lauschmann, H. (2008). Fractographic reconstitution of fatigue crack history - Part I. *FFEMS* 31 (2), 164–176. <https://doi.org/10.1111/j.1460-2695.2007.01211.x>.
- Qiu, H., Mori, H., Enoki, M., Kishi, T. (2000). Fracture mechanism and toughness of the welding heat-affected zone in structural steel under static and dynamic loading. *Metall. Mater. Trans. A*, 31 (11), 2785–2791. <https://doi.org/10.1007/BF02830338>.
- Salazar-Garrido, J.A., Terán-Gillén, J., García-Cerecero, G., Martínez-Madrid, M., Vargas-Arista, B. (2008). Metallurgical characterization of grain growth on weldment by SMAW process for a steel AISI 4140. *30th Congreso Internacional de Metalurgia y Materiales*, Saltillo, Coahuila, México, pp. 97–105.
- Shi, Y., Han, Z. (2008). Effect of weld thermal cycle on microstructure and fracture toughness of simulated heat-affected zone for a 800 MPa grade high strength low alloy steel. *J. Mater. Process. Tech.* 207 (1–3), 30–39. <https://doi.org/10.1016/j.jmatprotec.2007.12.049>
- Terán, M.G., Capula, C.S.I., Velázquez, J.C., Angeles-Herrera, D., Torres, S.E., Querios, B.A. (2017). Fracture toughness and Charpy CVN data for A36 steel with wet welding. *Soldagem Insp.* 22 (3), 258–268. <https://doi.org/10.1590/0104-9224/si2203.04>.
- Thewlis, G. (2004). Classification and quantification of microstructure in steels. *Mater. Sci. Tech.* 20 (2), 143–160. <https://doi.org/10.1179/026708304225010325>.
- UNE EN ISO 15609-1 (2004). *Specification and qualification of welding procedures for metallic materials. Part 1: Arc welding*. AENOR Spain, pp. 6–10.
- Wan, X.L., Wei, R., Wu, K.M. (2010). Effect of acicular ferrite formation on grain refinement in the coarse-grained region of heat-affected zone. *Mater. Charact.* 61 (7), 726–731. <https://doi.org/10.1016/j.matchar.2010.04.004>.